Supplemental Material for

"Fully Consistent DFT Determination of the Insulator-Metal Transition Boundary in Warm Dense Hydrogen"

Joshua Hinz[1], Valentin V. Karasiev[1]*, S. X. Hu[1], Mohamed Zaghoo[1], Daniel Mejía-Rodríguez[2], S.B. Trickey[2], and L. Calderín[3]

*vkarasev@lle.rochester.edu

[1] Laboratory for Laser Energetics, University of Rochester, Rochester, NY 14623

[2] Quantum Theory Project, Department of Physics, University of Florida, Gainesville, FL 32611

[3] Department of Materials Science and Engineering, University of Arizona, Tucson AZ 85721

17 August 2020

***Ab initio* simulations:**

Born-Oppenheimer molecular dynamic (BOMD) simulations were performed via the Vienna *ab initio* simulation package (VASP) [1-3] using the SCAN-L [4,5] exchange-correlation (XC) functional. The rVV10 [6,7] correlation correction was included in all simulations, unless specifically stated otherwise. Note that the rVV10 parametrization was set to include only the long-range interactions while preserving the description of the short and intermediate range interactions by SCAN-L. The motive is to incorporate the long-range van der Waals interaction that are not represented well by SCAN (or SCAN-L), despite its reasonable treatment in the vicinity of equilibrium bond lengths. Those long-range contributions may play an important role in H_2 dissociation. Note also that the *same* parametrization was used for both SCAN and SCAN-L.

All simulations used the NVT ensemble on a system of 256 non-spin-polarized atoms in a cubic super cell, with lattice parameters ranging from 7.05 to 10.27 Å. Electronic structures were calculated at the Γ point with 168 bands. Initial convergence tests at various thermodynamic conditions (see Fig. S1) indicated that use of Γ-point-only sampling introduces a maximum pressure uncertainty of 2.5%. Later convergence tests for a single isochore revealed a maximum pressure uncertainty of 5%. Each MD trajectory consists of 5000 to 6000 steps with a time step of 0.1 fs, giving a total simulation time of 0.5 to 0.6 ps. The bare ion Coulomb potential was

treated via the projector augmented wave (PAW) framework [8] with the use of PBE PAWs (metaGGA PAWs are not available in VASP at present).

Ring polymer path integral MD (PIMD) calculations for inclusion of nuclear quantum effects (NQEs) were done with the i-PI [9,10] interface to Quantum Espresso (QE) [11,12]. Those simulations used the SCAN [13] XC functional with the rVV10 van der Waals correction; see parametrization details above. Those calculations used a local pseudo-potential [14] while the rest of the technical parameter values were as consistent as possible with those used in the BOMD simulations. All MD simulation parameters are tabulated in Table S1 for reference.

With the exception of the 2500 and 3000 K IMT points, all other transition points were obtained from simulations along various isochores with densities ranging from 0.8 to 1.15 g/cm^3. This procedure was chosen so as to follow thermodynamic paths consistent with those in the static compression experiments. As a technical aside, as we moved along the isochore from low to high temperature, we took the initial snapshot from the previous temperature point in an attempt to converge the simulation faster by avoiding over-dissociated initial configurations. Furthermore, the isotherms in the low-pressure regime, which have a density range of 0.5 to 0.75 g/cm^3, were chosen because of the unknown steepness of the IMT boundary slope at the outset of this investigation.

As previously mentioned, the Γ point Brillouin zone sampling was used. While the effect of the Γ point on the pressure for the convergence checks was ≈2.5% error, it is important to check the effect on the resulting IMT boundary location. Figure S2 provides this comparison for 3 different *k*-point samplings (Γ point, Baldereschi mean value point (BMVP) and a 2x2x2 Monkhorst Pack *k*-mesh) in BOMD simulations along the 0.95 g/cm^3 isochore. It is clear that the slope change in pressure along the isochore is consistent with the onset of a dc conductivity of 2000 S/cm. With the use of Γ point sampling the slope change smoothens and the overall pressure along the isochore is increased by 2.5 to 5% relative to other k point samplings. While the sudden slope change in the pressure indicates a possible first order transition the use of the Γ point prevents us from confirming that speculation. Furthermore, the temperature location of the IMT boundary is shifted by 80 K. This fact suggests the Γ point will induce a systematic upward shift in the IMT boundary location. It should be noted that this temperature shift is equivalent to 2 to 3 error bars in the IMT temperature as obtained by the use of the dc conductivity to mark the transition, see

below. As such we view the effects of the Γ point to be relatively inconsequential for the purposes of this study.

Optical calculations:

The dynamic conductivity was calculated in the Kubo-Greenwood (KG) formalism [15,16] and the dc conductivity extracted in the static field limit. All KG calculations in the main text (BOMD and PIMD boundaries) were performed with VASP with the use of SCAN-L + rVV10 XC functional on a set of 20 evenly spaced snapshots from each MD trajectory. Note that the first 1000 steps of each trajectory were skipped prior to taking the snapshots for purposes of equilibration. The snapshot spacing was between 150 to 200 MD steps. The KG calculations used an automatically generated 2×2×2 Monkhorst-Pack *k*-mesh with a plane-wave energy cutoff of 1000 eV and 256 bands. Results of KG convergence tests for various thermodynamic conditions are shown in Fig. S3.

Because the calculated PIMD IMT boundary depends on use of SCAN + rVV10 to produce the ionic configurations and SCAN-L + rVV10 to generate the Kohn-Sham orbitals and eigenvalues for the calculated conductivity at each ionic configuration in the snapshot set, there might be concern about inconsistency. See discussion below.

The temperatures for which the average dc conductivity is directly above or below the 2000 S/cm criterion were identified. Linear interpolation between the two points then pinpointed the transition temperature at which a dc conductivity of 2000 S/cm occurred, Table S2 provides quick reference to our calculated transition temperatures and pressures. To estimate the uncertainty in the calculated IMT temperature, the standard error of the dc conductivity was added (or subtracted) from the dc conductivity for the two points in the fit and a reassessment of the transition temperature made. This procedure yields an estimated maximum uncertainty associated with how the IMT was calculated, of ± 30 K. However, this is not a direct measure of uncertainty from the theoretical approximations (primarily the XC approximation).

The corresponding reflectivity was calculated from the dynamical conductivity according to reference [17]. Figure S4 shows the dc conductivity and reflectivity at 1.96 eV (calculated relative to vacuum) for various isochores (some of which are not shown in the main text).

SCAN vs. SCAN-L:

As noted above and in the main text, use of SCAN in the PIMD simulations and SCAN-L in the KG calculations introduces an inconsistency in the calculated PIMD IMT boundaries. SCAN-L has been shown to reproduce, or nearly reproduce, various structural and energetic quantities from SCAN for solids [5] and molecules [4]. The inconsistency arises in part because of the inequivalence of the Kohn-Sham (KS) and generalized Kohn-Sham (gKS) schemes used to determine the ground state electronic structure [4,5]. For reasons of complexity and computational cost, SCAN calculations use gKS. SCAN-L calculations use KS. We did several calculations to quantify the effects of that difference.

First we calculated hydrogen dc conductivities (with QE KGEC [18]) from SCAN + rVV10 gKS orbitals and eigenvalues on the same set of ionic snapshots from the PIMD trajectories that we used with SCAN-L + rVV10 KS orbitals and eigenvalues in the KG calculations with VASP. The resulting transition temperature had an average increase of 11 K. *None* of the transition points had a shift greater than 20 K. This shift is smaller than the estimated methodological uncertainty; recall discussion above. As such, the difference between SCAN and SCAN-L (and the corresponding pseudo-potentials) inputs to the KG calculations of the PIMD boundary is inconsequential.

The second issue regarding the consistency of SCAN versus SCAN-L is the matter of the ionic trajectories and snapshots. That is, the comparison of PIMD and BOMD IMT boundaries includes both the direct electronic structure distinctions between SCAN and SCAN-L but also the possible direct NQEs. For a transition boundary that is clearly dependent on the ionic configuration set, even minor changes in its generation might have a significant impact on the IMT temperature. We quantify that effect next.

Figure S5 shows a direct comparison of the ionic pair correlation function (PCF) from SCAN-L + rVV10 and SCAN + rVV10 hydrogen BOMD simulations at 1.0 g/cm^3 and 900 K. It is clear that SCAN produces a system with smaller molecular character (height of the first peak) and molecules with a longer equilibrium bond length (position of first peak). Further calculations of the dc conductivity along the 0.8, 0.9 and 1.0 g/cm^3 isochores for BOMD simulations are shown in Fig. S6. Going from SCAN-L to SCAN to drive the BOMD simulation shifts the IMT boundary higher in temperature by 5 to 7% for all three isochores. Thus the shift in the IMT boundary associated with the inclusion of NQEs is underestimated by roughly 100 K (effective cancellation

of the two changes) when comparing the SCAN-L + rVV10 BOMD results to the PIMD SCAN + rVV10 results.

PBE comparison 3000 K:

As can be seen in Fig. 1 of the main text, the predicted IMT boundary from SCAN-L + rVV10 (BOMD) appears to approach that from PBE around 3000 K. To investigate this behavior further, the dc conductivities and the height of the first peak of the PCF from PBE and SCAN-L + rVV10 (both classical nuclei) along the 2500 K and 3000 K isotherms are compared in Fig. S7. At 3000 K, one sees clearly that the difference between PBE and SCAN-L + rVV10 results for both properties becomes significantly smaller than at lower temperatures across the whole density (or pressure) range of the isotherm. Furthermore, there is a striking similarity to the results from the two functionals for the overall structure of the curves of the two properties at 3000 K that does not appear in the comparison along the 2500 K isotherms. This finding helps support the notion that the predicted IMT boundaries of SCAN-L + rVV10 and PBE do in fact become close above 3000 K and that the two XC functionals predict a fluid hydrogen system with a similar level of accuracy at such thermodynamic conditions.

Further XC comparison:

Figure S8 shows a comparison of the optical and structural properties of the fluid hydrogen system for three different XC functionals (SCAN-L + rVV10, PBE, and vdW-DF1) along the 3000 K isotherm and the 0.8 g/cm^3 isochore for classical ions. Clearly all three XC functionals predict sudden increases of four or more orders of magnitude in the dc conductivity prior to reaching the 2000 S/cm criterion used to mark the IMT location. Furthermore, the IMT from SCAN-L + rVV10 lies between those from PBE and vdW-DF1 for both thermodynamic paths. That clearly is associated with how each XC functional captures (or does not) the molecular character of the system. This is an important feature as reference [19] suggests that the true IMT is most likely bounded by that of PBE and vdW-DF1 due to their respective under estimation of the metallization pressure and over stabilization of molecular hydrogen. It is clear from the analysis of the ionic pair correlation function that SCAN-L + rVV10 produces a molecular character (height of the first maximum) and corresponding average bond length (location of the first maximum) that consistently lies between PBE and vdW-DF1. This strongly suggests that the success of SCAN-L

across a wide range of systems, see [4,5], is transferable to this bulk fluid hydrogen system and provides an improved lower bound on the location of the IMT boundary.

HSE06 band gap comparison:

As noted in the main text, attention must be paid to the well-known underestimation of band gaps by semilocal XC functionals, particularly in the present context, the prediction of an insulator-to-metal transition. Because they have a single-determinant exchange contribution, hybrid functionals such HSE06 [20] can improve upon the band gap calculation of SCAN-L + rVV10. That improvement can be used to determine the effect of band-gap underestimation upon the predicted boundary location. With VASP, HSE06 band-gap calculations were done on the same PIMD SCAN + rVV10 ion configuration as was used in the SCAN-L + rVV10 band gap calculations. Convergence studies showed that a 4x4x4 Monkhorst-Pack *k*-mesh is required to calculate the band gap accurately. Such a restriction requires an exorbitant amount of computational time even for 20 snapshots at the relevant conditions. To avoid this, we have taken a single snapshot from the SCAN-L + rVV10 calculations that is closest to mean of the dc conductivity distribution to perform the HSE06 calculation, see Figure S9. The corresponding values have been tabulated and can be found in table S3.

It is clear that SCAN-L + rVV10 gave an underestimate of the indirect gap by a factor of 2 to 3 as compared to HSE06 in the insulating phase. *Crucially*, however, the closure of the two gaps is within 50 K of each other for both isochores; see Fig. S9. This difference is on the order of the error bar in the calculated transition temperature as determined by the dc conductivity criterion of 2000 S/cm. Thus, for the current sampling of the ion configuration space the underestimation of the band gap is inconsequential for the location of the gap closure. This further confirms the notion that it is the sampling of the ion configuration space that is most important in this problem. However, that is not to say that the underlying cause of the underestimated band gap does not effect the ion configuration space sampling; this requires a more detailed and systematic investigation.

Vibration/Rotational spectrum:

As an additional test for the disappearance of molecular character at the onset of metallization, we analyzed the vibrational/rotational spectrum. It can be obtained by taking the Fourier transform of the velocity auto-correlation function, namely

$$\text{vacf(t)} = \frac{1}{N}\sum_{i=1}^{N}\langle \vec{v}_i(t_o)\cdot\vec{v}_i(t)\rangle \quad (1)$$

Here N is the number of ions in the system, v_i is the velocity of the ith ion, t_o is the reference time used to start the calculation and the < > brackets indicate an average over t_o. Each calculation is performed across 350 MD steps (~120 fs) and consists of an average over 100 starting times such that each interval overlapped the preceding one by 300 MD steps. The first interval started at the 1000^{th} MD step. The corresponding vibrational/rotational spectrum can be attained through the Fourier transform of equation (1)

$$F\big(vacf(t)\big) = \int_{-\infty}^{\infty} vacf(t)e^{-i\omega t}dt \quad (2)$$

Results of the vacf calculation for 0.9 g/cm^3 (PIMD) and the real component of the transform are displayed in Figures S10a and S10b. At T_m=1150 K, the vacf indicated a significant jump in the minima at 10 and 30 fs. As observed from the vibrational/rotational spectrum, those changes lead to abrupt, clearly observable changes in all three peaks. This feature, coupled with the sudden drop in the first maximum of the ionic pair correlation function (PCF) at the onset threshold, 2000 S/cm, further strengthens the case for dissociation of molecular hydrogen as the key process in the metallization (The PCF analysis provides only the maximum number of possible molecules in the system, see discussion in Ref. [21]). Furthermore, the vibrational/rotational spectrum indicates a rapid increase at ω = 0 across the IMT temperature. This feature tends to appear across various isochores in the system, see Figure S10c, and becomes more gradual in the lower density limit, presumably as a possible critical point is approached. All of that is consistent with the previously discussed behavior of the dc conductivity, reflectivity, and PCF. It is not clear at present if this feature is directly related to a change in the rate of the velocity de-correlations (possibly due to dissociation) or to a change in the set of vibrational/rotational states.

1. G. Kresse, J. Hafner, *Ab Initio* molecular-dynamics simulation of the liquid-metal–amorphous-semiconductor transition in germanium. *Phys. Rev. B* **49**, 14251 (1994).
2. G. Kresse, J. Furthmüller, Efficiency of *ab-Initio* total energy calculations for metals and semiconductors using a plane-wave basis set. *Comput. Mater. Sci.* **6**, 15–50 (1996).

3. G. Kresse, J. Furthmüller, Efficient iterative schemes for *ab initio* total-energy calculations using a plane-wave basis set. *Phys. Rev. B* **54**, 11,169–11,186 (1996).
4. D. Mejía-Rodríguez, S. B. Trickey, Deorbitalization strategies for meta-generalized-gradient-approximation exchange-correlation functionals. *Phys. Rev. A* **96**, 052512 (2017).
5. D. Mejía-Rodríguez, S. B. Trickey, Deorbitalized meta-GGA exchange-correlation functionals in solids. *Phys. Rev. B* **98**, 115161 (2018).
6. O. A. Vydrov, T. Van Voorhis, Nonlocal van der Waals density functional: The simpler the better. *J. Chem. Phys.* **133**, 244103 (2010).
7. R. Sabatini, T. Gorni, S. de Gironcoli, Nonlocal van der Waals density functional made simple and efficient. *Phys. Rev. B* **87**, 041108 (2013).
8. G. Kresse, D. Joubert, From ultrasoft pseudopotentials to the projector augmented-wave method. *Phys. Rev. B* **59**, 1758–1775 (1999).
9. M. Ceriotti, J. More, D. E. Manolopoulos, i-PI: A python interface for ab initio path integral molecular dynamics simulations. *Comput. Phys. Commun.* **185**, 1019–1026 (2014).
10. V. Kapil *et al.*, i-PI 2.0: A universal force engine for advanced molecular simulations. *Comput. Phys. Commun.* **236**, 214–223 (2019).
11. P. Giannozzi *et al.*, QUANTUM ESPRESSO: A modular and open-source software project for quantum simulations of materials. *J. Phys.: Condens. Matter* **21**, 395502 (2009).
12. P. Giannozzi *et al.*, Advanced capabilities for materials modelling with quantum ESPRESSO. *J. Phys.: Condens. Matter* **29**, 465901 (2017).
13. J. Sun, A. Ruzsinszky, J. P. Perdew, Strongly constrained and appropriately normed semilocal density functional. *Phys. Rev. Lett.* **115**, 036402 (2015).
14. V.-V. Karasiev, T. Sjostrom, S.-B. Trickey, Generalized-gradient approximation noninteracting free energy functionals for orbital free density functional calculations, *Phys. Rev. B* **86**, 115101 (2012).
15. R. Kubo, Statistical-mechanical theory of irreversible processes. I. General theory and simple applications to magnetic and conduction problems. *J. Phys. Soc. Jpn.* **12**, 570–586 (1957).

16. D. A. Greenwood, The Boltzmann equation in the theory of electrical conduction in metals. *Proc. Phys. Soc. London* **71**, 585–596 (1958).
17. S. X. Hu *et al.*, Impact of first-principles properties of deuterium-tritium on inertial confinement fusion target designs. *Phys. Plasmas* **22**, 056304 (2015).
18. L. Calderín, V. V. Karasiev and S. B. Trickey, Kubo-Greenwood electrical conductivity formulation and implementation for projector augmented wave datasets, *Comput. Phys. Commun.* **221**, 118-142 (2017).
19. H. Y. Geng, Q. Wu, M. Marques, G. J. Ackland, Thermodynamic anomalies and three distinct liquid-liquid transitions in warm dense liquid hydrogen, *Phys. Rev. B* **100**, 134109
20. A. V. Krukau, O. A. Vydrov, A. F. Izmaylov, G. E. Scuseria, *J. Chem. Phys.* **125**, 224106 (2006).
21. V. Gorelov, C. Pierleoni, D. M. Ceperley, Benchmarking vdW-DF first-principles predictions against coupled electron–ion Monte Carlo for high-pressure liquid hydrogen. *Contrib. Plasma Phys.* **59**, e201800185 (2019).
22. H. Peng, Z.-H. Yang, J. P. Perdew, J. Sun, Versatile van der waals density functional based on a meta-generalized gradient approximation. *Phys. Rev. X* **6**, 041005 (2016).

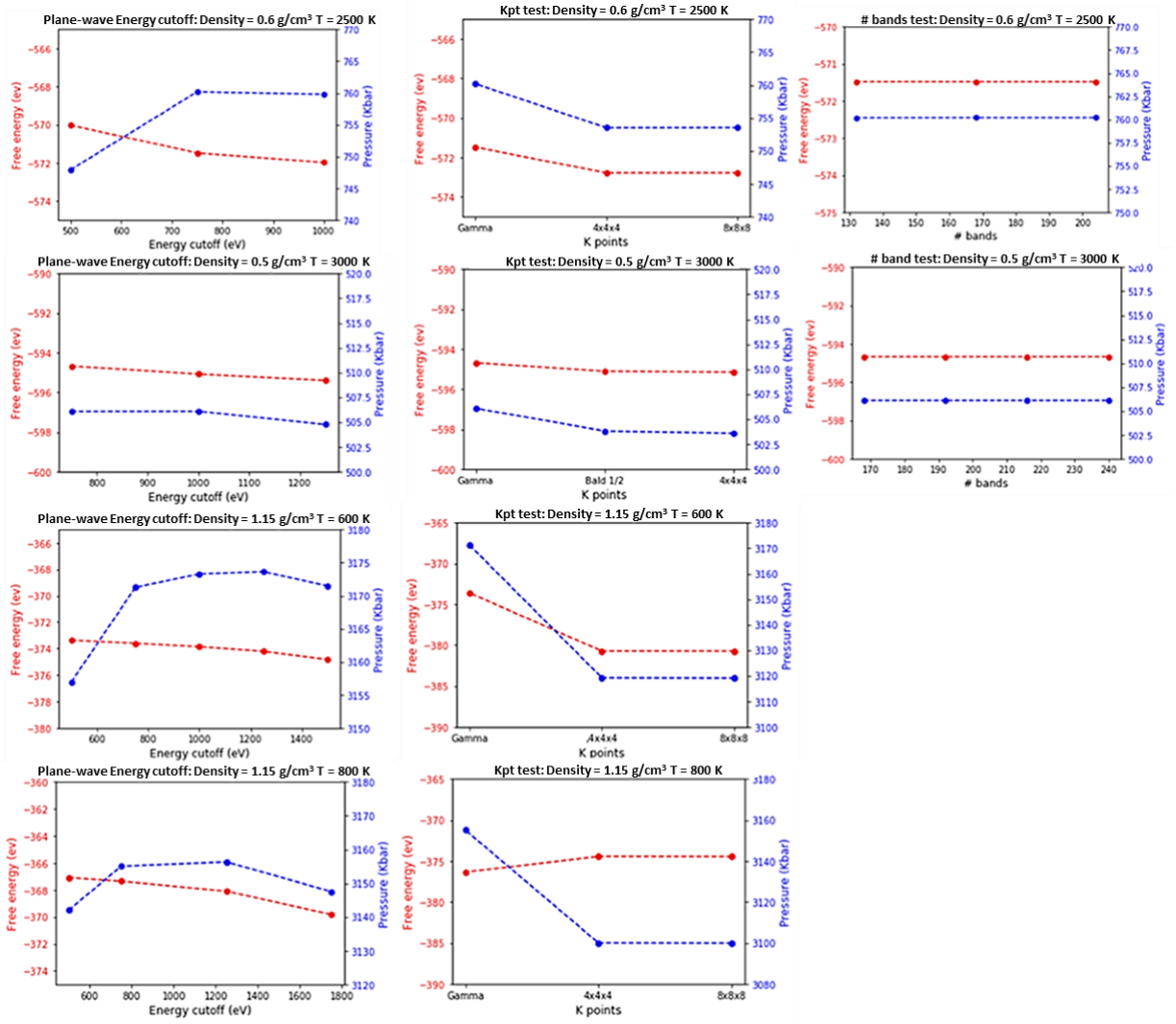

FIG. S1. Convergence tests performed by single point calculations for the setup of the MD simulation parameters including the plane –wave energy cutoff, *k*-mesh and number of bands. All red curves correspond to the free energy of the system (not including contribution from the ionic entropy) and blue curves correspond to the total pressure.

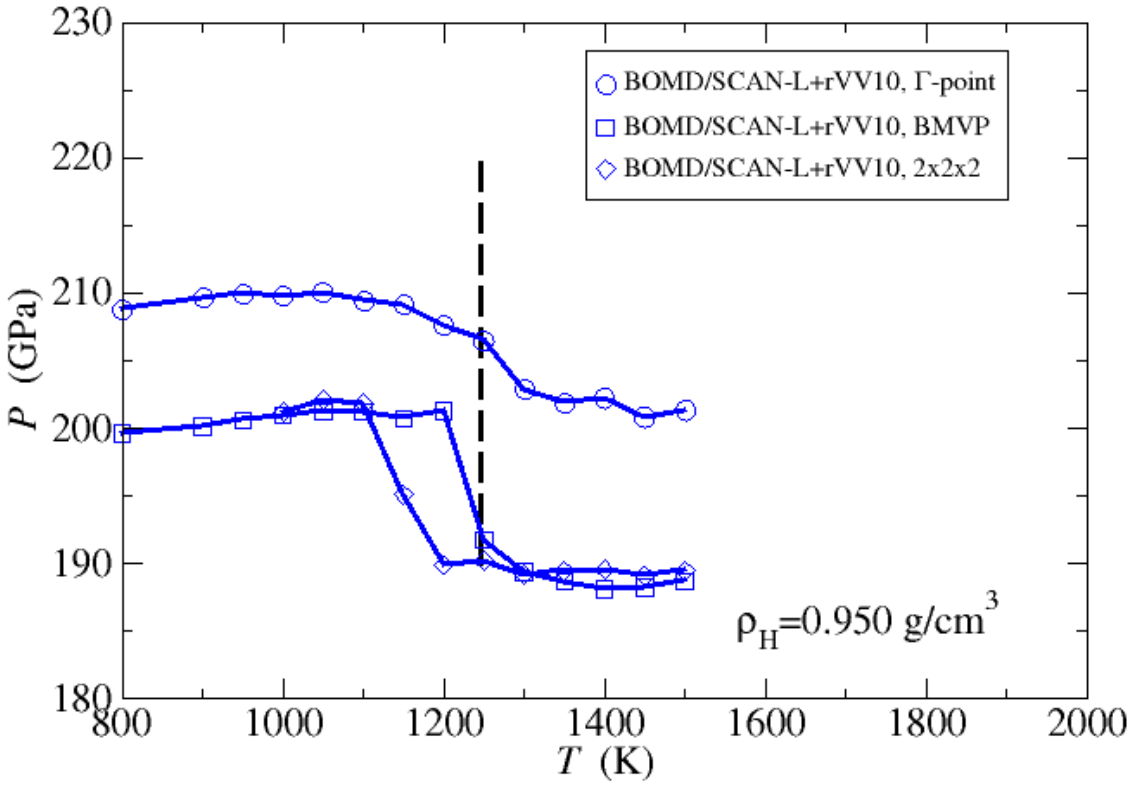

FIG. S2. *k*-point sampling comparison along the 0.95g/cm^3 isochore for H BOMD. Circles indicate the results with the Γ point, squares are the Baldereschi mean value point sampling and diamonds are for a 2x2x2 Monkhorst Pack grid. The vertical black dashed line indicates the location of the IMT for the Γ point case as based on the 2000 S/cm threshold for the dc conductivity.

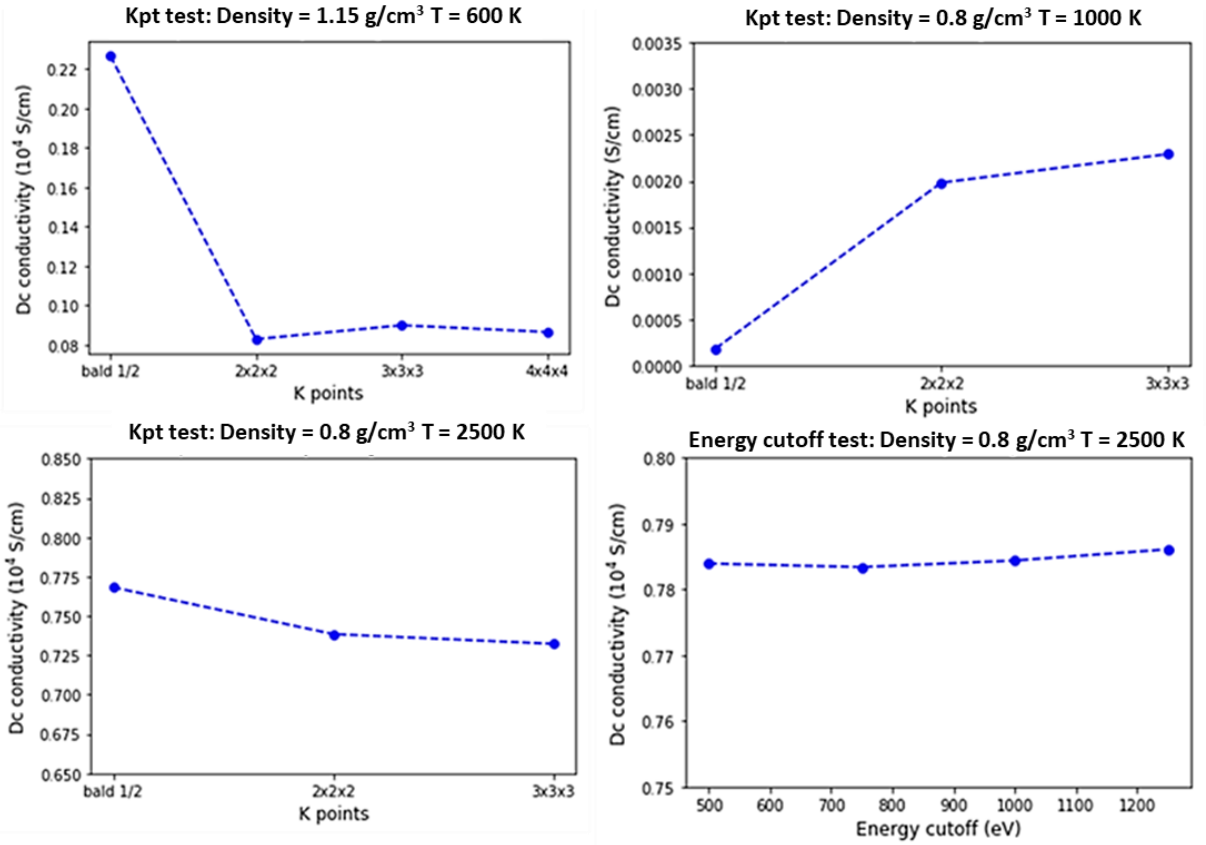

FIG. S3. Single snapshot calculations of the dc conductivity as a function of *k* points (top left and right and bottom left) and plane-wave energy cutoff (bottom right) used to determine the converged set of simulation parameters for the dc conductivity calculations over the set of snapshots for each thermodynamic condition.

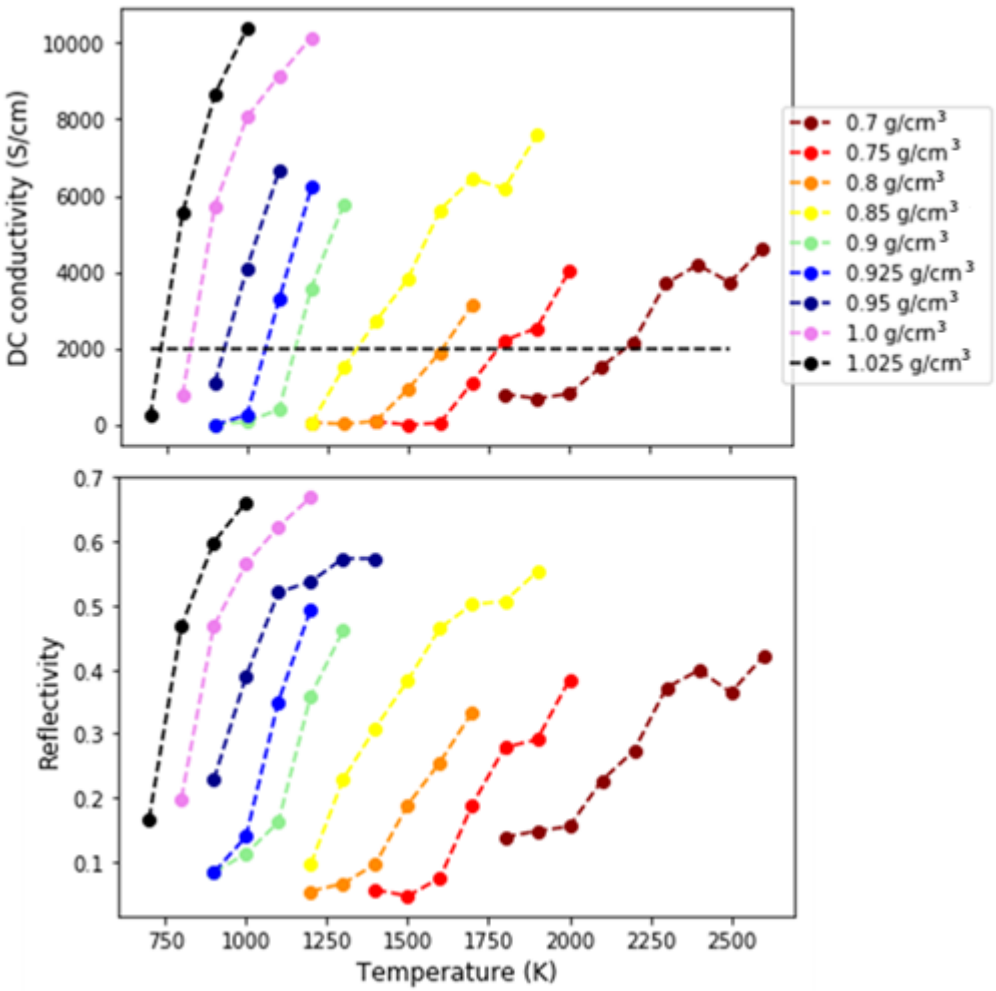

FIG. S4. The dc conductivity (top) and reflectivity (bottom) of the PIMD isochores with the use of SCAN-L + rVV10 in the KG calculation. Note the horizontal dotted black line in the dc conductivity panel: it indicates the 2000 S/cm criterion used to determine the IMT.

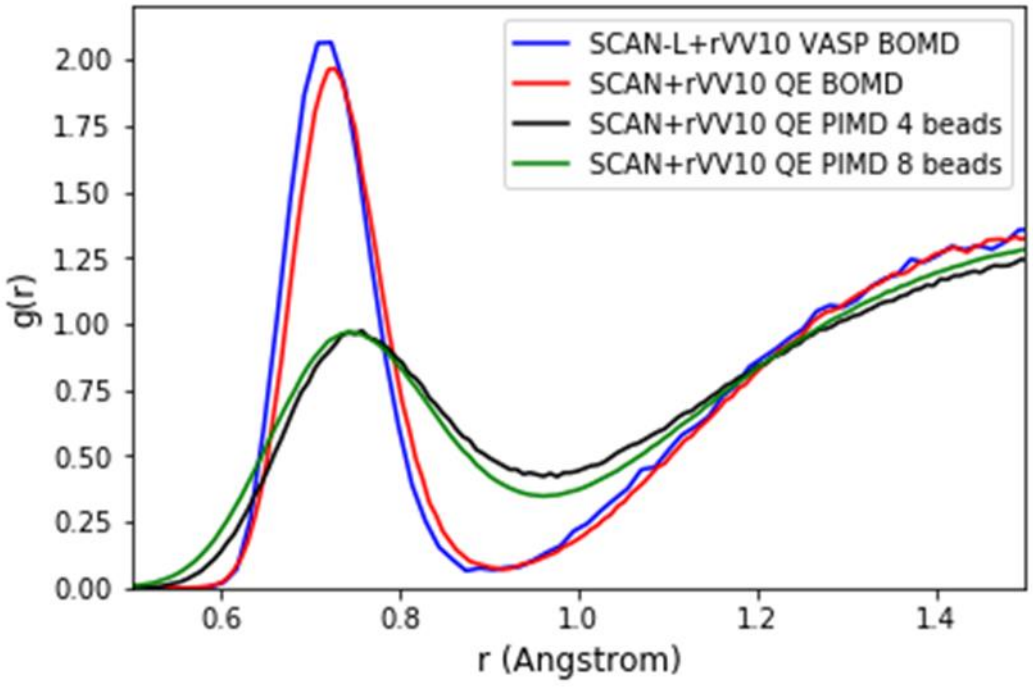

FIG. S5. Pair correlation function (PCF) for four separate simulations of hydrogen at 1.0 g/cm^3 and 900 K. Blue curve corresponds to the BOMD simulation with VASP using SCAN-L + rVV10. Red curve is the PCF from PIMD simulation with one bead (i.e. BOMD) using SCAN + rVV10. Green and black are PCFs from PIMD simulations with eight and four beads respectively.

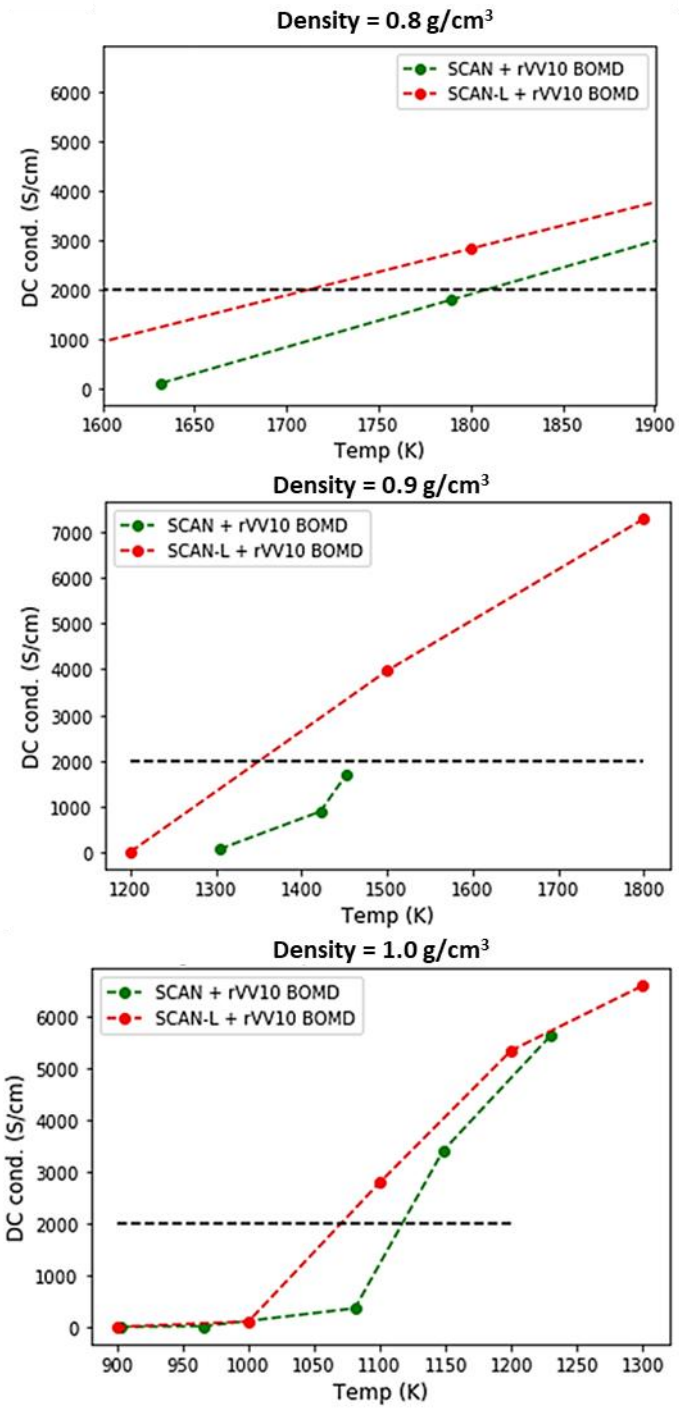

FIG. S6. Comparison of dc conductivities along the 0.8 (top), 0.9 (middle), and 1.0 g/cm^3 (bottom) isotherms. Note SCAN-L + rVV10 is used in all of the KG calculations. The dotted black line indicates a dc conductivity of 2000 S/cm. Each red curve corresponds to the BOMD simulation with the use of SCAN-L + rVV10. Each green curve corresponds to BOMD simulations with SCAN + rVV10. Note that the KG calculations for both sets of data were performed with SCAN-L + rVV10.

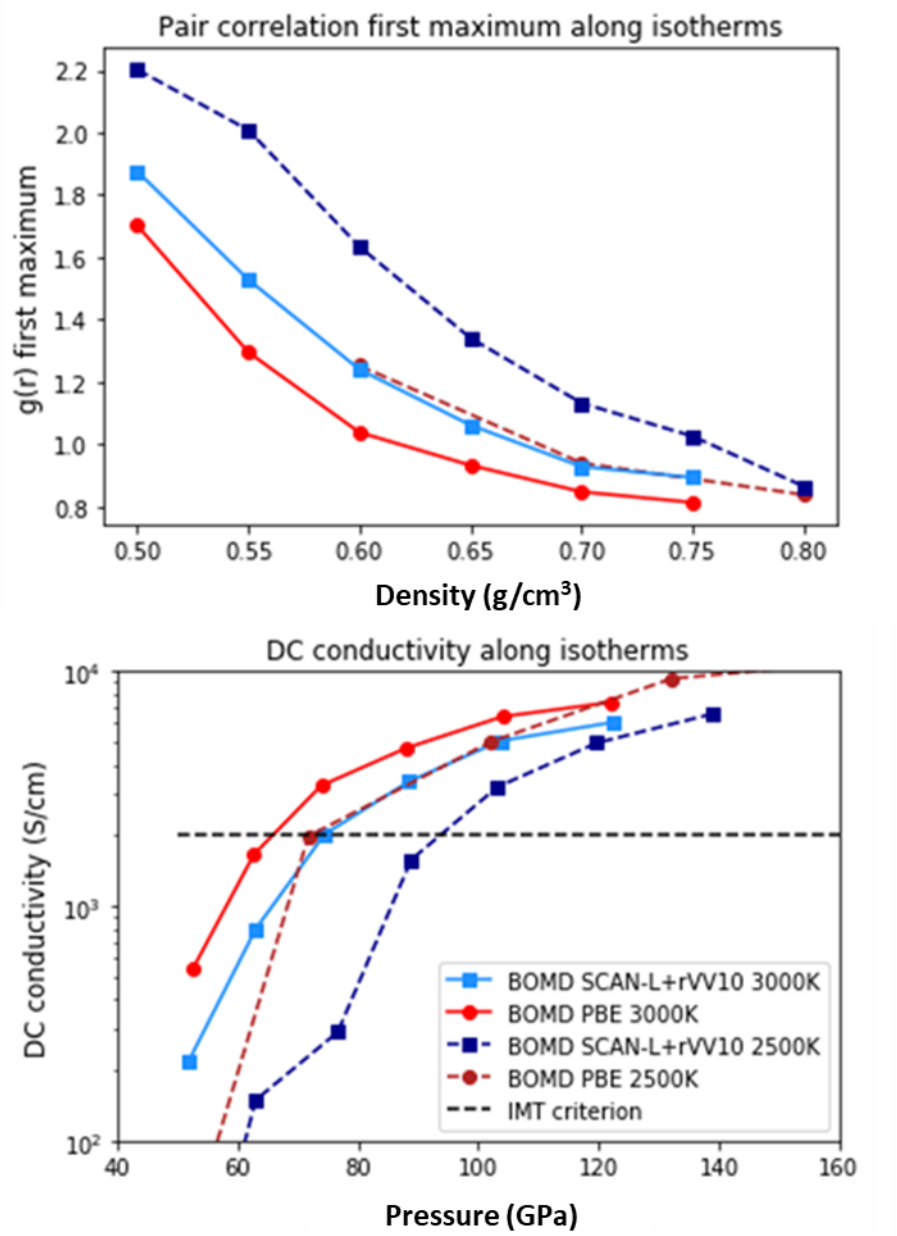

FIG. S7. Top, first peak of the pair correlation function for the corresponding dc conductivity curves in the bottom panel. Bottom, comparison of the dc conductivity along the 2500K and 3000K isotherms for SCAN-L + rVV10 and PBE (BOMD).

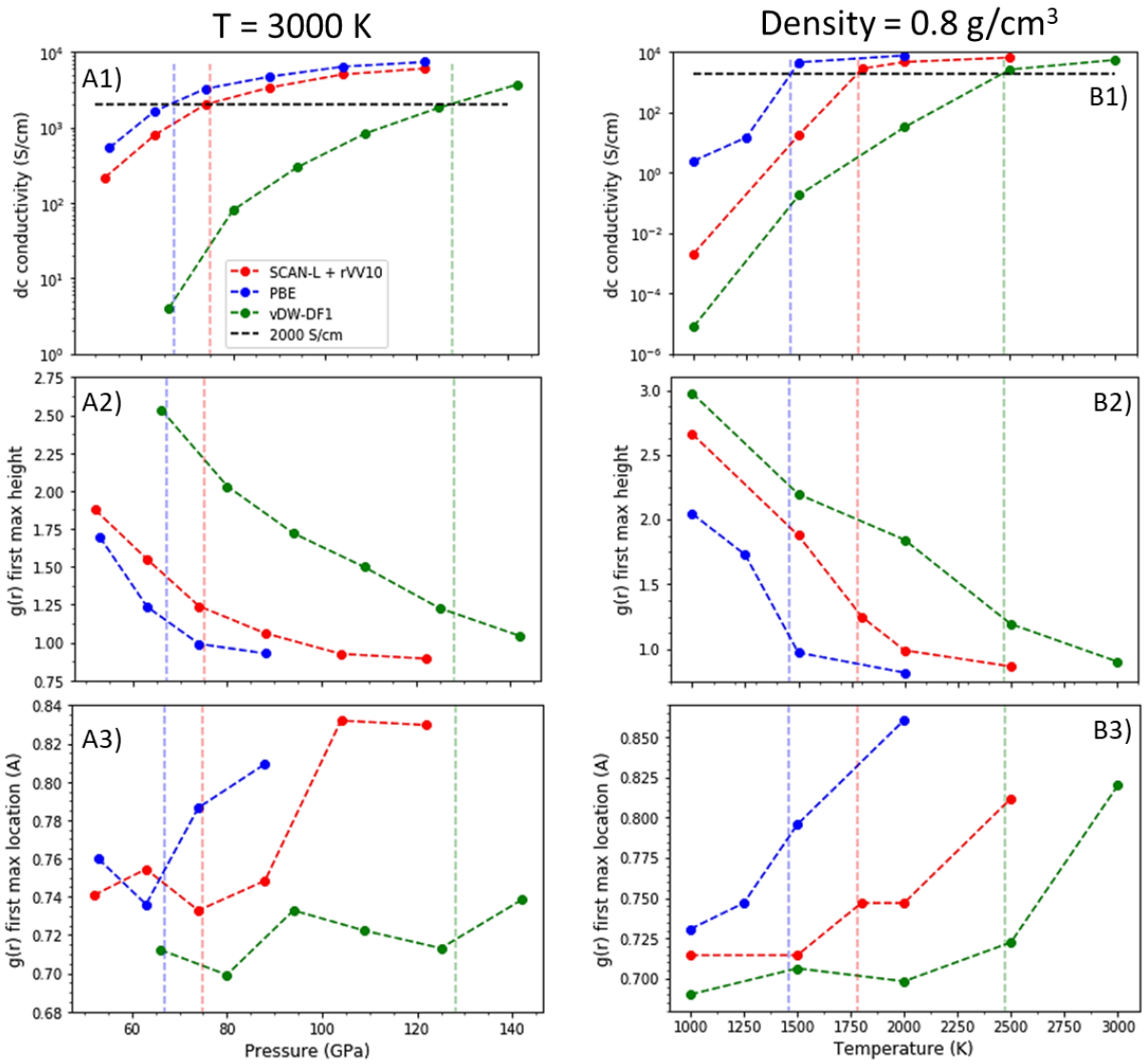

FIG. S8. (Left) Panel A1 is the dc conductivity comparison along the 3000 K isotherm for SCAN-L + rVV10 (red), PBE (blue), and vdW-DF1 (green). The dotted black line indicates a dc conductivity threshold, 2000 S/cm, used as the primary criterion to mark the IMT. The corresponding dashed vertical lines indicate the pressure at which 2000 S/cm is reached along the isotherm for the correspondingly colored XC functional. Panel A2 gives the height of the first peak of the pair correlation function along the isotherm. Panel A3 gives the corresponding location of the first peak of the pair correlation function. (Right). Panel B1 shows the dc conductivity along the 0.8 g/cm^3 isochore again for the three XC functionals with the same coloring as in the figure key. Panels B2 and B3 are the respective heights and positions of the first maximum of the pair correlation function along the isochore.

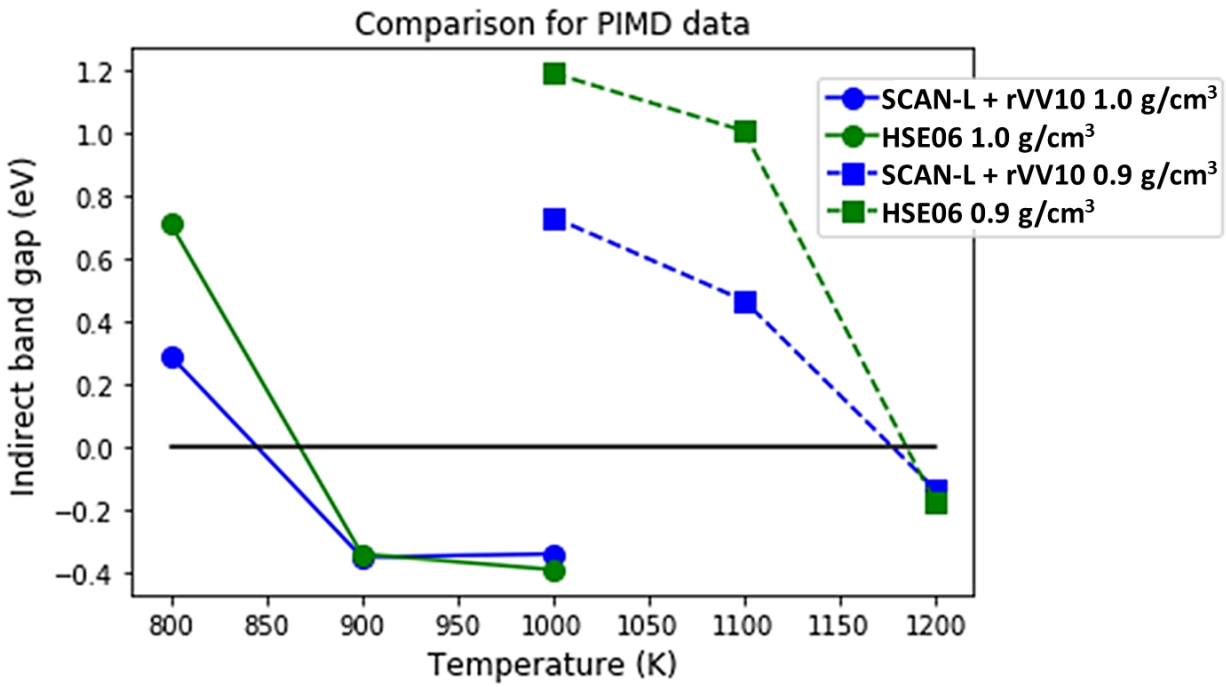

FIG. S9. Comparison of the SCAN-L + rVV10 and HSE06 indirect band gaps for the 1.0 g/cm^3 (circles) and 0.9 g/cm^3 (squares) isochores calculated on snapshots from PIMD simulations.

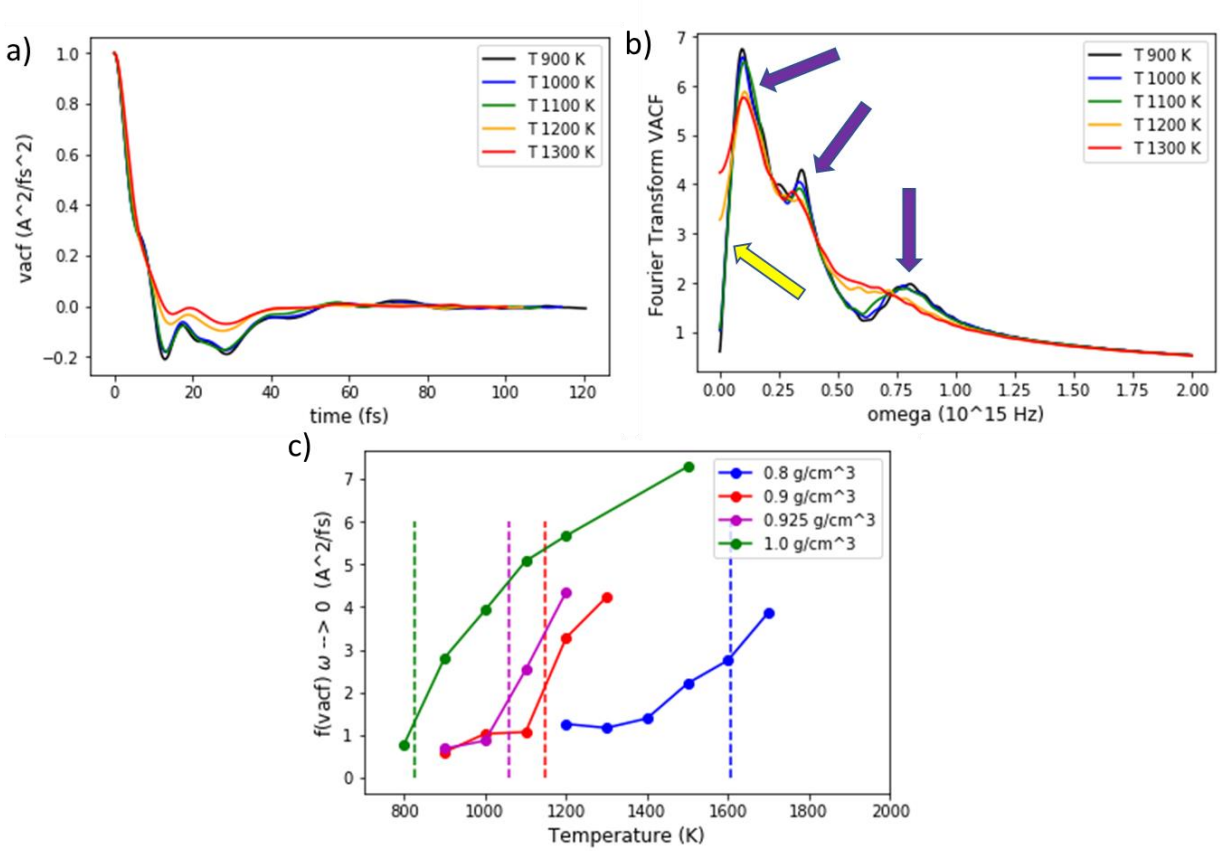

FIG. S10. (a) Vacf along the 0.9 g/cm^3 isochore. Note the IMT temperature is 1150 K, precisely when changes around 20 fs become most pronounced. (b) Real part of the Fourier transform of the vacf in (a). At the metallization temperature there is a significant change in all three peaks as indicated by the blue arrows and correspondingly at $\omega = 0$ (yellow arrow). (c) Change in the vibrational/rotational spectrum at $\omega = 0$ for various isochores from PIMD simulations. The vertical dashed lines represent the IMT temperature of the isochore as defined by the 2000 S/cm criterion.

TABLE S1. Quick reference for the parameters used in the BOMD and PIMD simulations. The Fermi smearing temperature is set to the ionic temperature to be maintained by the thermostat.

Parameter	BOMD	PIMD
# atoms	256	256
Plane-Wave cutoff energy	750 eV	2700 eV
Convergence criterion on the total electronic free energy	1E-5 eV	2.7E-5 eV
# bands	168	160
K pt's	Gamma	Gamma
Time step	0.1 fs	0.2 to 0.5 fs (adjust for temperature and density)
# MD steps	6000	6000
Electron partial occupancies	Fermi smearing	Fermi smearing
Bare proton treatment	Projector Augmented Wave potentials [8]	Local [14]
Ensemble	NVT	NVT
Thermostat	Nosé-Hoover (acts every 40 MD steps)	Andersen (acts every 10 MD steps)
# beads	N.A.	8
rVV10 b parameter value (see [22] for details)	15.7	15.7

TABLE S2. Quick reference for the calculated IMT points as based on the minimum dc conductivity threshold of 2000 S/cm. Note the BOMD calculated boundary was obtained with the use of SCAN-L + rVV10, while the PIMD boundary was found with SCAN + rVV10 in the molecular dynamics phase of the calculations. All calculations reported here used SCAN-L + rVV10 in the optics calculations.

BOMD H/D		**PIMD H**		**PIMD D**	
P (GPa)	**T (K)**	**P (GPa)**	**T (K)**	**P (GPa)**	**T (K)**
74	3000	106	2174	107	2270
95	2500	123	1788	124	1959
141	1711	143	1607	164	1523
184	1351	163	1341	186	1255
208	1246	186	1150	211	1108
232	1070	199	1057	224	964
260	986	209	930	236	953
316	735	235	825	249	857
		250	733		

TABLE S3. Tabulated values for the band gap comparison of FIG S9.

Density (g/cm^3)	Temperature (K)	SCAN-L + rVV10 indirect band gap (eV)	HSE06 indirect band gap (eV)
1.0	800	0.2922	0.7106
1.0	900	-0.3544	-0.3412
1.0	1000	-0.3468	-0.3854
0.9	1000	0.7309	1.1891
0.9	1100	0.4663	1.0047
0.9	1200	-0.1343	-0.1767